Modelling Simul. Mater. Sci. Eng. **17** (2009) 075013 (13pp) doi:10.1088/0965-0393/17/7/075013

# Viscoelastic effect on acoustic band gaps in polymer-fluid composites

**B Merheb[1,4], P A Deymier[1], K Muralidharan[1], J Bucay[1], M Jain[2,5], M Aloshyna-Lesuffleur[2], R W Greger[3], S Mohanty[2] and A Berker[2]**

[1] Department of Materials Science and Engineering, The University of Arizona, Tucson, AZ 85721, USA
[2] 3M Co., Corporate Research Materials Laboratory, Bldg. 201-3N-04, 3M Center, St. Paul, MN 55144-1000, USA
[3] Volt Services Group, 3M Center, 3M Corporate Research Materials Laboratory, St. Paul, MN 55144-1000, USA

E-mail: deymier@email.arizona.edu

Received 26 February 2009, in final form 21 July 2009
Published 22 September 2009
Online at stacks.iop.org/MSMSE/17/075013

**Abstract**

In this paper, we present a theoretical analysis of the propagation of acoustic waves through elastic and viscoelastic two-dimensional phononic crystal structures. Numerical calculations of transmission spectra are conducted by extending the finite-difference-time-domain method to account for linear viscoelastic materials with time-dependent moduli. We study a phononic crystal constituted of a square array of cylindrical air inclusions in a solid viscoelastic matrix. The elastic properties of the solid are those of a silicone rubber. This system exhibits very wide band gaps in its transmission spectrum that extend to frequencies in the audible range of the spectrum. These gaps are characteristic of fluid matrix/air inclusion systems and result from the very large contrast between the longitudinal and transverse speeds of sound in rubber. By treating the matrix as a viscoelastic medium within the standard linear solid (SLS) model, we demonstrate that viscoelasticity impacts the transmission properties of the rubber/air phononic crystal not only by attenuating the transmitted acoustic waves but also by shifting the passing bands frequencies toward lower values. The ranges of frequencies exhibiting attenuation or frequency shift are determined by the value of the relaxation time in the SLS model. We show that viscoelasticity can be used to decrease the frequency of pass bands (and consequently stop bands) in viscoelastic/air phononic crystals.

(Some figures in this article are in colour only in the electronic version)

[4] Author to whom any correspondence should be addressed.
[5] Present addresses: Institute for Computational Engineering and Science, University of Texas, Austin, TX 78712, USA and Department of Physics, University of California, Berkeley, CA 94720, USA.

  

## 1. Introduction

The problem of the formation of spectral gaps in the propagation of elastic waves in phononic crystals has attracted a great deal of attention in the past decade [1–6]. Phononic crystals are composed of two- or three-dimensional periodic repetitions of some inclusions inside a matrix where the matrix and inclusions can be constituted of solids or fluids. Band gaps result from Bragg scattering of acoustic waves by the periodic array of inclusions in the matrix. It is known that the existence of band gaps depends on the contrast in the (i) physical and elastic properties of the inclusions and matrix materials and (ii) the filling fraction of inclusions and the geometry of the array and inclusions [1–6]. Spectral gaps at low frequency can be obtained in the case of arrays with large periods (and large inclusions) and materials with low speed of sound. Elastic fluid/fluid acoustic band-gap (ABG) materials have been shown to possess band gaps at significantly lower frequencies than their solid/solid and solid/fluid counterpart [2] due, in part, to the absence of transverse polarization. Another approach to achieve low-frequency gaps uses structures composed of heavy inclusions coated with a soft material, which possess resonances, the so-called locally resonant materials [6]. Although the frequency of resonance can be very low (two orders of magnitude below the Bragg frequency), the associated band gaps are narrow and in order to achieve broad stop bands, one resorts to superposing different resonant structures.

Extensive literature exists on the acoustic properties of elastic phononic crystals, while in contrast, only limited information is available concerning the properties of phononic crystals composed of viscoelastic materials. The most relevant works on such materials include those of Psarobas [7] and Liu *et al* [8]; Psarobas theoretically demonstrated the existence of an absolute band gap in the transmission spectrum of a three-dimensional sonic crystal composed of viscoelastic spherical inclusions in air, with the simple Kelvin–Voigt model being used to model the viscoelastic medium. In the more recent work by Liu *et al* [8] two-dimensional (2D) phononic crystals consisting of aluminum cylinders in a rubber matrix were examined using a finite-difference-time-domain (FDTD) method in conjunction with a Kelvin–Voigt model with fractional derivatives, to include both dispersive and dissipative viscoelastic effects.

The impact of viscoelasticity on the properties of phononic crystals is receiving increasing attention and new theoretical tools that can account for dissipation have been recently implemented. For instance a plane wave expansion (PWE) method for the calculation of the band structure of phononic crystals that accounts for both propagative and evanescent waves has been developed [9]. In the common PWE method, the equation for the propagation of elastic waves in an inhomogeneous medium is replaced by an Eigen value problem in the frequency at fixed wave vectors. With the new PWE method, one converts the equations of wave propagation to an Eigen value problem in the complex wave vectors at fixed frequency. Dissipation and viscoelasticity can therefore be incorporated by employing complex and frequency-dependent elastic moduli.

Within this context, this paper aims at exploring and characterizing the acoustic properties of phononic crystals consisting of viscoelastic materials using a FDTD method. In the field of phononic crystals, the FDTD method complements the PWE method in that it can account for finite size systems as well as calculate transmission coefficients. Specifically, we consider 2D ABG structures composed of an array of cylinders of air inclusions in a solid elastic/viscoelastic rubber matrix, whose properties are chosen to reflect that of commercially available polysilicone rubber, where the transverse speed of sound is at least one order of magnitude smaller than that of the longitudinal speed of sound. This could lead to the presence of wide band gaps at low frequencies similar to the well-known water/air structures [2]. Thus, in this work, using the FDTD method, we model and characterize the transmission properties

of air/rubber ABG structures as a function of its viscoelasticity in conjunction with its band-gap properties. In addition, we develop an analytic formulation capable of predicting the effects of viscoelasticity on the frequency-dependent response of ABG systems.

While the moduli of linear elastic materials are independent of frequency, linear viscoelastic materials have dynamic moduli that generally decrease with decreasing frequency. The mechanical response of viscoelastic materials will therefore vary over time providing a dissipative mechanism that is absent in linear elastic materials, in addition to already-existing dispersive responses. In this work, viscoelasticity is introduced through a compressible linear viscoelastic solid constitutive relation, with its time-dependent modulus given by the standard linear solid (SLS) model. Numerical calculations of transmission through viscoelastic media are conducted by extending the FDTD method to account for time-dependent moduli. This viscoelastic FDTD method is introduced and described in detail in section 2. In the results (section 3) we show that the elastic rubber/air ABG structures with centimeter dimensions exhibit very wide band gaps extending to low frequencies. Moreover we show that, by changing the viscoelastic characteristics of the material, the transmission spectrum differs significantly from the behavior of linear elastic materials. Viscoelasticity impacts the transmission spectrum by attenuating transmission but also by shifting the passing bands of the structure toward lower frequencies. The conclusions drawn from this study are reported in section 4.

## 2. Theoretical analysis, methods and models

The study of the propagation of waves in inhomogeneous media is a long-standing area of interest in many fields of application. The FDTD method for elastic composite media is well documented [10] and not described in this paper. However, in this section, we describe, in detail, an efficient FDTD method that accounts for viscoelasticity within a SLS model. In a second subsection we describe the model phononic structure used in this paper.

### *2.1. Mathematical models*

The elastic wave equation is given by

$$\frac{\partial \boldsymbol{v}}{\partial t} = \frac{1}{\rho}\mathrm{div}\boldsymbol{\sigma}, \tag{1}$$

where $t$ is time, $\rho$ is the mass density, $\boldsymbol{v}(t)$ is the velocity vector and $\sigma$ is the total stress tensor.

To calculate the stress tensor we employ the constitutive equation for the general linear viscoelastic fluid (GLVF). When the GLVF material is compressible, the total stress tensor is given by

$$\sigma(t) = 2\int_{-\infty}^{t} G\left(t-t'\right)\boldsymbol{D}(t')\mathrm{d}t' + \int_{-\infty}^{t}\left[K\left(t-t'\right) - \frac{2}{3}G\left(t-t'\right)\right]\left[\nabla \bullet \boldsymbol{v}(t')\right]\boldsymbol{I}\mathrm{d}t', \tag{2}$$

where $\boldsymbol{D}(\boldsymbol{x}, t)$ is the rate of deformation tensor given by

$$\boldsymbol{D} = \tfrac{1}{2}\left[(\nabla \boldsymbol{v}) + (\nabla \boldsymbol{v})^{\mathrm{T}}\right] \tag{3}$$

and $G(t)$ and $K(t)$ are the steady shear and bulk moduli, respectively. These moduli can be experimentally determined through rheometry and the data can be fit in a variety of ways, including the use of mechanical-analog models. A viscoelastic model, or in effect, the behavior pattern it describes, may be illustrated schematically by combinations of springs and dashpots, representing elastic and viscous factors, respectively. Hence, a spring is assumed to reflect the properties of an elastic deformation, and similarly a dashpot to depict the characteristics of viscous flow. Clearly, the simplest manner in which to schematically construct a viscoelastic

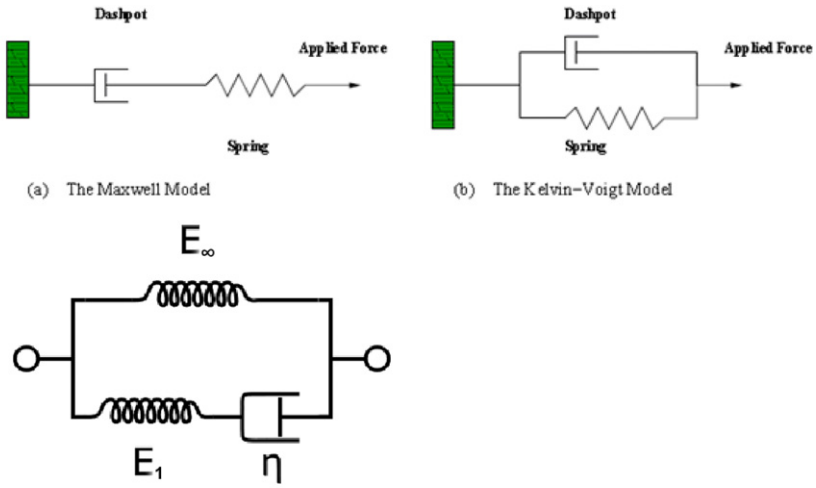


(a) The Maxwell Model (b) The Kelvin–Voigt Model

(c) The Standard Linear Solid model

**Figure 1.** Spring and dashpot illustration of the Maxwell, Kelvin–Voigt and the SLS models.

model is to combine one of each component either in series or in parallel. These combinations result in the two basic models of viscoelasticity, the Maxwell and the Kelvin–Voigt models, respectively. Their schematic representations are displayed in figures 1(*a*) and (*b*). Another simple viscoelastic model is the SLS model presented in figure 1(*c*), which accounts for both creep and stress in its representation.

In this paper we focus on the SLS model where the steady extensional modulus $E(t)$ is defined as

$$E(t) = E_\infty + E_1 \mathrm{e}^{-t/\tau}, \tag{4}$$

where $\{E_1\ ,\ \tau\}$ are the modulus and relaxation time of the dashpot and $E_\infty = E(\infty)$ is the infinite time extensional modulus.

By introducing $\alpha(t)$ as a function having the same form as $E(t)$:

$$\alpha(t) = \alpha_0 + \alpha_1 \mathrm{e}^{-t/\tau}, \tag{5}$$

where

$$\alpha_0 = \frac{E_\infty}{E_{\mathrm{sum}}}, \qquad \alpha_1 = \frac{E_1}{E_{\mathrm{sum}}}, \qquad \alpha_0 + \alpha_1 = 1 \text{ and } E_{\mathrm{sum}} = E_\infty + E_1$$

We obtain

$$E(t) = E_{\mathrm{sum}}\alpha(t). \tag{6}$$

In the limit of a large relaxation time, that is, in the absence of viscosity (i.e. the absence of dashpot), $\alpha(t) = 1$ and the extensional modulus becomes $E(t) = E_{\mathrm{sum}}$. This is the elastic limit of the SLS model whereby the effective elastic modulus of the rubber is the sum of the moduli of two springs in parallel.

To find the additional moduli, we assume that

$$E(t) = 2G(t)(1 + \upsilon) = 3K(t)(1 - 2\upsilon), \tag{7}$$

with

$$\begin{aligned} G(t) &= G_{\mathrm{sum}}\alpha(t) \\ K(t) &= K_{\mathrm{sum}}\alpha(t), \end{aligned} \tag{8}$$

and

$$\begin{aligned} G_{\text{sum}} &= \mu \\ K_{\text{sum}} - \tfrac{2}{3} G_{\text{sum}} &= \lambda. \end{aligned} \tag{9}$$

In the above equations, $\nu$ is Poisson's ratio and $\lambda$ and $\mu$ are the Lamé constant and shear modulus, respectively. Note that the elastic behavior is recovered for $\alpha_0 = 1 (\alpha_1 = 0)$.

Now we consider a 2D elastic/viscoelastic material, where the system is infinite in the vertical direction $z$, and none of its properties depend on $z$ (translational invariance). In this case the non-zero Cartesian components of the 2D stress tensor become

$$\sigma_{xx}(t) = 2\int_{-\infty}^{t} G\left(t-t'\right)\frac{\partial v_x}{\partial x}(t')\mathrm{d}t' + \int_{-\infty}^{t}\left(K\left(t-t'\right) - \frac{2}{3}G\left(t-t'\right)\right)\left(\frac{\partial v_x}{\partial x}(t') + \frac{\partial v_y}{\partial y}(t')\right)\mathrm{d}t', \tag{10}$$

$$\sigma_{yy}(t) = 2\int_{-\infty}^{t} G\left(t-t'\right)\frac{\partial v_y}{\partial y}(t')\mathrm{d}t' + \int_{-\infty}^{t}\left(K\left(t-t'\right) - \frac{2}{3}G\left(t-t'\right)\right)\left(\frac{\partial v_x}{\partial x}(t') + \frac{\partial v_y}{\partial y}(t')\right)\mathrm{d}t', \tag{11}$$

$$\sigma_{xy}(t) = \sigma_{yx}(t) = \int_{-\infty}^{t} G\left(t-t'\right)\left(\frac{\partial v_x}{\partial y}(t') + \frac{\partial v_y}{\partial x}(t')\right)\mathrm{d}t'. \tag{12}$$

For the sake of illustration, let us insert equation (6) into (10). Using $C_{11} = 2\mu + \lambda$, $C_{12} = \lambda$ and $C_{44} = \mu$, $\sigma_{xx}(t)$ becomes

$$\begin{aligned} \sigma_{xx}(t) = {} & \alpha_0 C_{11}\frac{\mathrm{d}u_x}{\mathrm{d}x}(t) + \alpha_0 C_{12}\frac{\mathrm{d}u_y}{\mathrm{d}y}(t) \\ & + \alpha_1 C_{11}\mathrm{e}^{-t/\tau}\int_{-\infty}^{t}\mathrm{e}^{t'/\tau}\frac{\partial v_x}{\partial x}(t')\mathrm{d}t' + \alpha_1 C_{12}\mathrm{e}^{-t/\tau}\int_{-\infty}^{t}\mathrm{e}^{t'/\tau}\frac{\partial v_y}{\partial y}(t')\,\mathrm{d}t'. \end{aligned} \tag{13}$$

Alternatively, to avoid integration, we first differentiate equation (13) with respect to time:

$$\begin{aligned} \frac{\partial \sigma_{xx}}{\partial t}(t) = {} & \alpha_0 C_{11}\frac{\partial v_x}{\partial x}(t) + \alpha_0 C_{12}\frac{\partial v_y}{\partial y}(t) \\ & + \alpha_1 C_{11}\left[\frac{-1}{\tau}\int_{-\infty}^{t}\mathrm{e}^{-(t-t')/\tau}\frac{\partial v_x}{\partial x}(t')\mathrm{d}t' + \mathrm{e}^{-t/\tau}\mathrm{e}^{t/\tau}\frac{\partial v_x}{\partial x}(t)\right] \\ & + \alpha_1 C_{12}\left[\frac{-1}{\tau}\int_{-\infty}^{t}\mathrm{e}^{-(t-t')/\tau}\frac{\partial v_y}{\partial y}(t')\mathrm{d}t' + \mathrm{e}^{-t/\tau}\mathrm{e}^{t/\tau}\frac{\partial v_y}{\partial y}(t)\right]. \end{aligned} \tag{14}$$

Incorporating equation (13) into equation (14), we obtain

$$\frac{\partial \sigma_{xx}}{\partial t}(t) = C_{11}\frac{\partial v_x}{\partial x}(t) + C_{12}\frac{\partial v_y}{\partial y}(t) - \frac{1}{\tau}\left[\sigma_{xx}(t) - \alpha_0 C_{11}\frac{\partial u_x}{\partial x}(t) - \alpha_0 C_{12}\frac{\partial u_y}{\partial y}(t)\right]. \tag{15}$$

By doing the same calculations for $\sigma_{yy}$ and$\sigma_{xy}$ we obtain

$$\frac{\partial \sigma_{yy}}{\partial t}(t) = C_{11}\frac{\partial v_y}{\partial y}(t) + C_{12}\frac{\partial v_x}{\partial x}(t) - \frac{1}{\tau}\left[\sigma_{yy}(t) - \alpha_0 C_{11}\frac{\partial u_y}{\partial y}(t) - \alpha_0 C_{12}\frac{\partial u_x}{\partial x}(t)\right], \tag{16}$$

$$\frac{\partial \sigma_{xy}}{\partial t}(t) = C_{44}\left(\frac{\partial v_x}{\partial y}(t) + \frac{\partial v_y}{\partial x}(t)\right) - \frac{1}{\tau}\left[\sigma_{xy}(t) - \alpha_0 C_{44}\left(\frac{\partial u_x}{\partial y}(t) + \frac{\partial u_y}{\partial x}(t)\right)\right]. \tag{17}$$

### *2.2. Finite difference methods*

We can now develop the FDTD method for the SLS Model. This involves transforming the governing differential equations in the time domain into finite differences and solving them as one progresses in time in small increments. These equations constitute the basis for the implementation of the FDTD in 2D viscoelastic systems. For the implementation of the FDTD method we divide the computational domain into $N_x \times N_y$ sub domains (grids) with dimension $\mathrm{d}x$, $\mathrm{d}y$. For space derivatives we use central differences, where the y direction is staggered to the $x$ direction. For the time derivative we use forward difference, with a time interval $\mathrm{d}t$.

Using expansions at point $(i, j)$ and time $(n)$, equation (1), in component form, becomes

$$v_x^{n+1}(i, j) = v_x^n(i, j) + \frac{\mathrm{d}t}{\rho(i, j)}\left(\frac{\sigma_{xx}^{n+1}(i, j) - \sigma_{xx}^{n+1}(i-1, j)}{\mathrm{d}x} + \frac{\sigma_{xy}^{n+1}(i, j) - \sigma_{xy}^{n+1}(i, j-1)}{\mathrm{d}y}\right), \tag{18}$$

$$v_y^{n+1}(i, j) = v_y^n(i, j) + \frac{\mathrm{d}t}{\rho(i+1/2, j+1/2)} \times \left(\frac{\sigma_{yy}^{n+1}(i, j+1) - \sigma_{xx}^{n+1}(i, j)}{\mathrm{d}y} + \frac{\sigma_{xy}^{n+1}(i+1, j) - \sigma_{xy}^{n+1}(i, j)}{\mathrm{d}x}\right), \tag{19}$$

where we define $\rho(i+1/2, j+1/2) = \sqrt[4]{\rho(i, j)\rho(i+1, j)\rho(i, j+1)\rho(i+1, j+1)}$,

The stress component $\sigma_{xx}$ is calculated by discretizing equation (15), using expansion at point $(i, j)$ and time $(n)$.

$$\sigma_{xx}^{n+1}(i,j) = \frac{1}{\left(1+\dfrac{\mathrm{d}t}{\tau(i,j)}\right)}\left[\sigma_{xx}^{n}(i,j) + \mathrm{d}t\left(\begin{array}{l} \dfrac{C_{11}(i+1/2,j)}{\alpha_0(i+1/2,j)}\dfrac{v_x^n(i+1,j)-v_x^n(i,j)}{\mathrm{d}x} \\ +\dfrac{C_{12}(i+1/2,j)}{\alpha_0(i+1/2,j)}\dfrac{v_y^n(i,j)-v_y^n(i,j-1)}{\mathrm{d}y} \\ +\dfrac{1}{\tau(i,j)}C_{11}(i+1/2,j)\dfrac{u_x^n(i+1,j)-u_x^n(i,j)}{\mathrm{d}x} \\ +\dfrac{1}{\tau(i,j)}C_{12}(i+1/2,j)\dfrac{u_y^n(i,j)-u_y^n(i,j-1)}{\mathrm{d}y} \end{array}\right)\right]. \tag{20}$$

We define

$$C_{11}(i+1/2, j) = \sqrt{C_{11}(i+1, j)C_{11}(i, j)},$$
$$C_{12}(i+1/2, j) = \sqrt{C_{12}(i+1, j)C_{12}(i, j)}$$

and

$$\alpha_0(i+1/2, j) = \sqrt{\alpha_0(i+1, j)\alpha_0(i, j)}.$$

Similarly, the components $\sigma_{yy}$ and $\sigma_{xy}$ are obtained in discretized form:

$$\sigma_{yy}^{n+1}(i,j) = \frac{1}{\left(1+\frac{\mathrm{d}t}{\tau(i,j)}\right)}\left[\sigma_{yy}^{n}(i,j) + \mathrm{d}t\left(\begin{array}{l} \dfrac{C_{11}(i+1/2,j)}{\alpha_0(i+1/2,j)}\dfrac{v_y^n(i,j)-v_y^n(i,j-1)}{\mathrm{d}y} \\ +\dfrac{C_{12}(i+1/2,j)}{\alpha_0(i+1/2,j)}\dfrac{v_x^n(i+1,j)-v_x^n(i,j)}{\mathrm{d}x} \\ +\dfrac{1}{\tau(i,j)}C_{11}(i+1/2,j)\dfrac{u_y^n(i,j)-u_y^n(i,j-1)}{\mathrm{d}y} \\ +\dfrac{1}{\tau(i,j)}C_{12}(i+1/2,j)\dfrac{u_x^n(i+1,j)-u_x^n(i,j)}{\mathrm{d}x} \end{array}\right)\right], \tag{21}$$

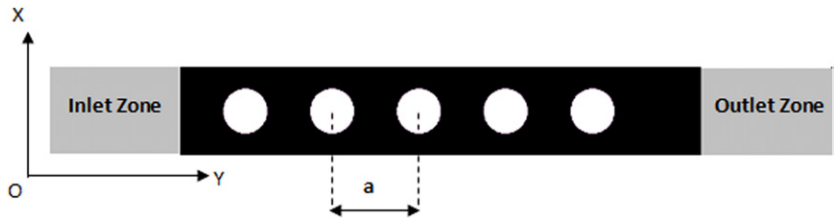


**Figure 2.** 2D cross section of the FDTD model structure with a square array of air cylinders embedded in a rubber matrix, lattice parameter $a = 12$ mm and cylinder diameter $d = 8$ mm; the cylinders are parallel to the $Z$-axis of the Cartesian coordinate system ($OXYZ$).

$$\sigma_{xy}^{n+1}(i,j) = \frac{1}{\left(1+\frac{\mathrm{d}t}{\tau(i,j)}\right)} \times \left[\begin{array}{l} \sigma_{xy}^{n}(i,j) + \mathrm{d}t\dfrac{C_{44}\,(i,\,j+1/2)}{\alpha_0\,(i,\,j+1/2)}\left(\dfrac{v_x^n(i,\,j+1)-v_x^n(i,\,j)}{\mathrm{d}y}+\dfrac{v_y^n(i,\,j)-v_y^n\,(i-1,\,j)}{\mathrm{d}x}\right) \\ +\mathrm{d}t\dfrac{C_{44}\,(i,\,j+1/2)}{\tau(i,\,j)}\left(\dfrac{u_x^n(i,\,j+1)-u_x^n(i,\,j)}{\mathrm{d}y}+\dfrac{u_y^n(i,\,j)-u_y^n\,(i-1,\,j)}{\mathrm{d}x}\right) \end{array}\right], \tag{22}$$

where $C_{44}(i,\,j+1/2) = \sqrt{C_{44}(i,\,j+1)C_{44}(i,\,j)}$ and $\alpha_0(i,\,j+1/2) = \sqrt{\alpha_0(i,\,j+1)\alpha_0(i,\,j)}$.

It has to be mentioned that the above way of discretizing the equations ensures second order accurate central difference for the space derivatives. The field components $u_x$ and $u_y$ have to be centered in different space points.

The FDTD method for elastic and viscoelastic media is local in space and ideally suited for computer simulation on parallel platforms. All the calculations reported in this paper were performed on at least eight parallel processors.

### *2.3. Structure*

The model structure studied in this paper, as illustrated in figure 2, is composed of three separate regions. The central region is a phononic crystal modeled as an array of isotropic cylindrical inclusions with circular cross section, embedded in an isotropic material matrix. The cylinders, of diameter $d$, are assumed to be parallel to the $Z$-axis of the Cartesian coordinates ($XYZ$). The array is then considered infinite in the two directions $X$ and $Z$ and finite in the direction of propagation of the probing wave ($Y$). The periodicity along the direction $X$ is ensured by the application of periodic boundary conditions. The matrix is made of rubber and the inclusions are made of air. For all calculations reported here, the physical characteristics of the rubber are those of a polysilicone rubber of mass density $= 1260\,\mathrm{kg\,m^{-3}}$, longitudinal speed $C_l = 1200\,\mathrm{m\,s^{-1}}$ and transverse speed $= 20\,\mathrm{m\,s^{-1}}$. These values were obtained from experimental measurements. In particular the longitudinal speed of sound was determined by measuring the time of flight of a longitudinal acoustic pulse. The transverse speed of sound was calculated from the measurement of the shear modulus of the rubber using a torsion balance. The measured values are consistent with other values reported in the literature for other rubber materials [11]. Air is modeled as a fluid of mass density $= 1.3\,\mathrm{kg\,m^{-3}}$ and longitudinal speed $C_l = 340\,\mathrm{m\,s^{-1}}$. The air cylinders have a diameter of 8 mm and are arranged on a $6 \times 1$ square array with a lattice parameter $a = 12$ mm.

For the calculations that include the effect of viscoelasticity, we vary $\alpha_0$ between 1 and 0.25 and the relaxation time $\tau$ between $10^{-2}$ and $10^{-9}$ s. The phononic crystal region is sandwiched

between 2 homogeneous regions called the inlet and outlet regions, respectively, as shown in figure 2. These regions (20 mm in width) have the same density and speed of sound as the matrix material of the phononic crystal and are made elastic ('$\alpha_0 = 1$ and $\alpha_1 = 0$') in order to apply the Mur absorbing boundary conditions [10] at the extreme ends of these regions. Note that in the case of a phononic crystal with a viscoelastic matrix the interface between the elastic inlet and outlet regions and the viscoelastic matrix leads to some minor reflections of acoustic waves, which are negligible for all practical purposes.

A stimulus sound wave packet taking the form of a Gaussian-modulated cosine waveform is launched in the inlet region. The displacement amplitude of the stimulus is $10^{-6}$ m and is oriented along the $Y$ direction, to ensure that the wave packet has a longitudinal polarization. This wave packet corresponds to a broadband signal with a chosen central frequency of 350 kHz, enabling the study of the transmission of phononic crystals from audible to ultrasonic frequencies. The time step $\mathrm{d}t$ (see equation (23)) is chosen to satisfy an enhanced Courant stability criterion that ensures stability of the algorithm for the calculations with viscoelastic media.

$$\mathrm{d}t = \mathrm{Min}\left\{\frac{1}{16}\sqrt{\frac{1}{\left(\frac{C_1^i}{\mathrm{d}x}\right)^2 + \left(\frac{C_1^i}{\mathrm{d}y}\right)^2}}\right\}, \tag{23}$$

where $C_1^i$ is the longitudinal speed of sound for the medium $i$ (1, 2, 3)- inlet, phononic crystal and outlet regions, respectively.

All the calculations reported in this paper are for $\mathrm{d}x = \mathrm{d}y = 10^{-4}$ m and $\mathrm{d}t = 7.4$ ns.

The total simulation time for the calculation of the transmission spectra is chosen to exceed 0.02 s, which is sufficient to obtain reliable transmission coefficients.

## 3. Results and discussion

In this section, we report the results of our simulations examining the effect of viscoelasticity on the properties of the rubber/air system by the extended FDTD method. Several simulations were carried out on the 2D array of air cylinders embedded in a viscoelastic silicone rubber matrix (presented in figure 2) with various values of the viscoelastic coefficients, namely $\alpha_0$ and the relaxation time $\tau$ that determine the level of viscosity of the rubber.

In figure 3 we report the calculated transmission coefficient corresponding to different values of $\alpha_0$: $\alpha_0 = 1$, which corresponds to the elastic case (black solid line), $\alpha_0 = 0.75$ (blue — - —), $\alpha_0 = 0.5$ (green - - -) and finally $\alpha_0 = 0.25$ (red $\cdots$) with a relaxation time $\tau$ equal to $10^{-4}$ s. The transmission coefficient is calculated as the ratio of the spectral power transmitted in the composite to that transmitted in an elastic homogeneous medium composed of the matrix material. The inset of figure 3 presents a zoom on the high frequency region. First we notice that the transmission spectrum corresponding to the elastic structure ($\alpha_0 = 1$, black solid line) shows two band gaps where the transmission coefficient approaches zero. The wider gap ranges from approximately 3 to 87 kHz; the second gap is from 90 to 125 kHz.

These band gaps are reminiscent of those reported in [2] for a water/air phononic crystal. The large contrast between the longitudinal and transverse speeds of sound in rubber leads to a separation of modes with different polarization. When stimulated with a longitudinal wave packet, the rubber/air phononic crystal behaves in all respects as a fluid-like rubber/air system.

In addition, we notice that as the matrix becomes more viscoelastic through a decreasing $\alpha_0$, the low-frequency passing bands are attenuated. In addition, their frequencies shift to lower values. In contrast, the high frequency passing bands are only attenuated with no noticeable frequency shift for very low relaxation times. In order to quantify these effects, we plot in

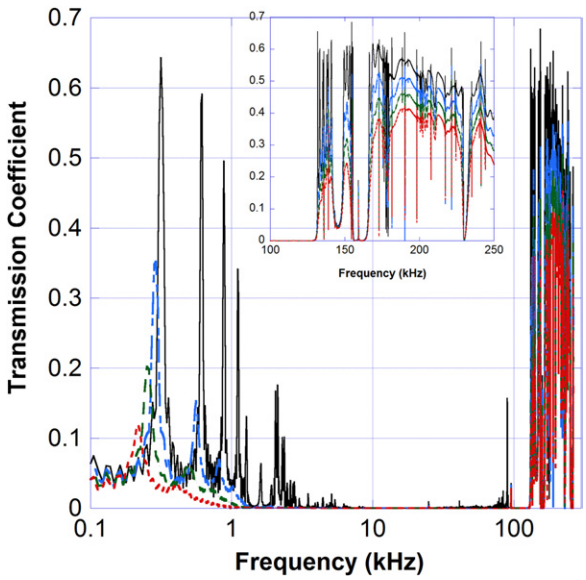


**Figure 3.** Transmission coefficients of the rubber matrix air inclusions system considering the rubber as: an elastic medium (black solid line, $\alpha_0 = 1$), a viscoelastic medium with: $\alpha_0 = 0.75$ (blue — - —), $\alpha_0 = 0.5$ (green - - -) and finally $\alpha_0 = 0.25$ (red $\cdots$) with a relaxation time $\tau$ equal to $10^{-4}$ s.

figure 4((*a*)–(*d*)) the transmission coefficient (a measure of the amount of attenuation) and the frequency for two different narrow passing bands as functions of $\alpha_0$ for several values of $\tau$ ($\tau = 10^{-8}$ s: black round symbol; $\tau = 10^{-6}$ s: blue lozenge symbol; $\tau = 10^{-4}$ s: red square symbol; $\tau = 10^{-2}$ s: green triangle symbol). In the absence of viscoelasticity ($\alpha_0 = 1$), these bands are located at the low frequency of 320 Hz and at the high frequency of 141 kHz. The effect of relaxation time on attenuation and frequency of the passing bands is not monotonic. For instance in figure 4(*c*) the transmission coefficient of the high frequency band reaches its minimum value for a relaxation time $\tau = 10^{-6}$ s. This transmission coefficient decreases drastically and reaches a value of zero beyond $\alpha_0 = 0.75$. The transmission coefficient remains constant for the long relaxation time $\tau = 10^{-2}$ s and decreases but remains finite for all $\alpha_0$ for $\tau = 10^{-4}$ or $10^{-8}$ s. The behavior of the transmission coefficient for the low-frequency passing band is also not a monotonic function of $\tau$ (figure 4(*a*)). When $\alpha_0$ decreases from 1 to 0.25, the attenuation of the low passing band reaches its maximum for $\tau = 10^{-4}$ s with only small differences in the values of the transmission coefficient for the other three relaxation times.

In figure 4(*b*), we notice that the band originally at 320 Hz shifts toward lower frequencies when $\alpha_0$ decreases for a relaxation time $\tau$ smaller than $10^{-2}$ s. For $\tau = 10^{-2}$ s the frequency of this band does not change. In a similar way, there is no frequency shift with decreasing $\alpha_0$ of the high frequency band (141 kHz for $\alpha_0 = 1$) for $\tau$ larger than or equal to $10^{-6}$ s. However, for the very small relaxation time $\tau = 10^{-8}$ s, the band shifts toward lower frequencies (figure 4(*d*)).

To shed some light on the effect of viscoelasticity on the frequency of narrow passing bands, we model the narrow band as the vibrational mode associated with material with a linear mass density, $m$, attached to a 1D SLS model. The frequency-dependent complex elastic modulus of the SLS is given by

$$E^*(\omega) = E_\infty + \frac{1}{(1/E_1) - (\mathrm{i}/\eta\omega)}. \tag{24}$$

The viscous coefficient $\eta$ is defined in terms of the relaxation time and modulus as $E_1\tau$.

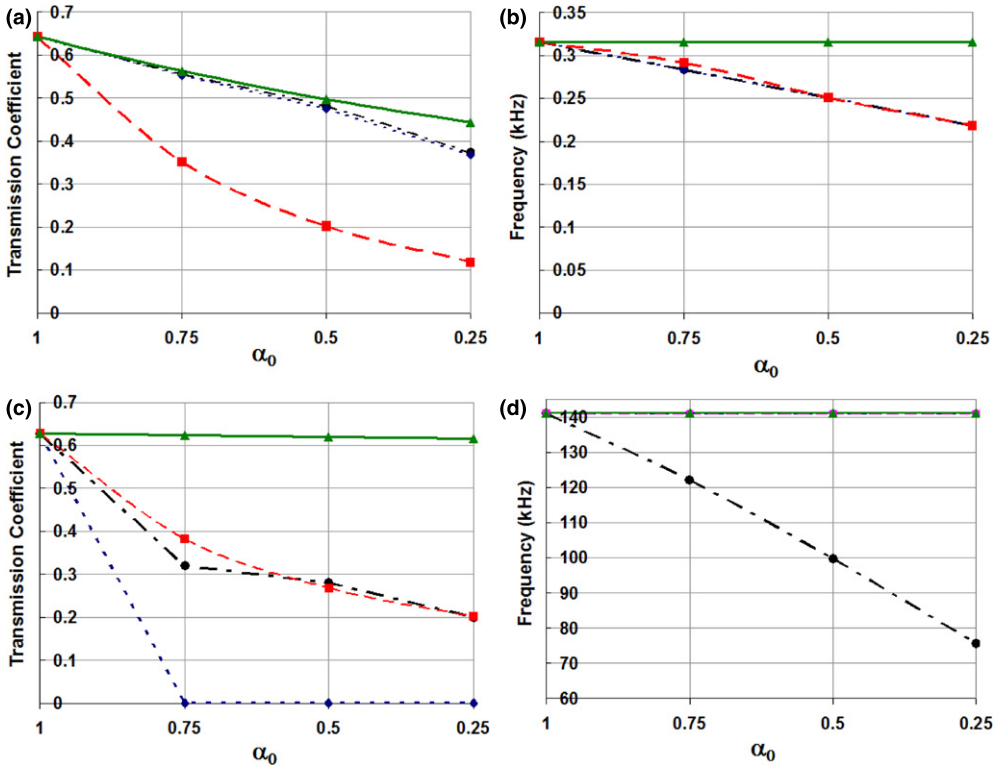


**Figure 4.** Attenuation and frequency of low frequency (320 Hz) (*a*), (*b*) and high frequency (141 kHz) (*c*), (*d*) bands as a function of $\alpha_0$ for four values of $\tau$ ($\tau = 10^{-8}$ s: black round symbol; $\tau = 10^{-6}$ s: blue lozenge symbol; $\tau = 10^{-4}$ s: red square symbol; $\tau = 10^{-2}$ s: green triangle symbol).

The equation of motion of the mass-SLS system in the frequency domain can be written as

$$m\omega^2 = E^* = E_\infty + \frac{1}{(1/E_1) - (\mathrm{i}/\eta\omega)}. \tag{25}$$

Equation (25) can be rewritten in the form of a third order equation in the complex plane

$$\omega^3 - \frac{\mathrm{i}E_1}{\eta}\omega^2 - \frac{E_\infty + E_1}{m}\omega + \frac{\mathrm{i}E_\infty E_1}{m\eta} = 0. \tag{26}$$

Introducing $\alpha_0 = \frac{E_\infty}{E_{\mathrm{sum}}}$, $E_{\mathrm{sum}} = E_\infty + E_1$ and $\tau$, equation (26) becomes

$$\omega^3 - \frac{\mathrm{i}}{\tau}\omega^2 - \frac{E_{\mathrm{sum}}}{m}\omega + \mathrm{i}\frac{\alpha_0 E_{\mathrm{sum}}}{m.\tau} = 0. \tag{27}$$

Equation (27) possesses three complex solutions that can be written in the form

$$\omega^* = \omega_{\mathrm{real}}\,(\alpha_0, \tau, E_{\mathrm{sum}}) + \mathrm{i}\,\omega_{\mathrm{imag}}\,(\alpha_0, \tau, E_{\mathrm{sum}}) \tag{28}$$

It is convenient to rewrite the equation of motion (27) with simplified parameters:

$$\omega^3 - \mathrm{i}b\omega^2 - c\omega + \mathrm{i}d = 0 \tag{29}$$

with $b = 1/\tau$; $c = E_{\mathrm{sum}}/m$; $d = \alpha_0 E_{\mathrm{sum}}/m\tau$

The analytical solutions of this equation are

$$\begin{aligned}
\omega_1 &= \frac{\mathrm{i}b}{3} - \frac{2^{1/3}\left(b^2 - 3c\right)}{3\delta^{1/3}} + \frac{\delta^{1/3}}{3.2^{1/3}},\\
\omega_2 &= \frac{\mathrm{i}b}{3} + \frac{\left(1 + \mathrm{i}\sqrt{3}\right)\left(b^2 - 3c\right)}{3.2^{2/3}\delta^{1/3}} - \frac{\left(1 - \mathrm{i}\sqrt{3}\right)\delta^{1/3}}{6.2^{1/3}},\\
\omega_3 &= \frac{\mathrm{i}b}{3} + \frac{\left(1 - \mathrm{i}\sqrt{3}\right)\left(b^2 - 3c\right)}{3.2^{2/3}\delta^{1/3}} - \frac{\left(1 + \mathrm{i}\sqrt{3}\right)\delta^{1/3}}{6.2^{1/3}}\\
&\text{with } \delta = -2\mathrm{i}b^3 + 9\mathrm{i}bc - 27\mathrm{i}d + 3\sqrt{3}\sqrt{b^2c^2 - 4c^3 - 4b^3d + 18bcd - 27d^2}.
\end{aligned} \tag{30}$$

It is straightforward to verify that in the absence of viscoelasticity (i.e. very large $\tau$ and $b = d = 0$), $\omega_1 = 0$, $\omega_2 = -\sqrt{c}$ and $\omega_3 = \sqrt{c}$. The latter solution corresponding to the well-known frequency of a mass/elastic spring system, namely $\omega_{\text{elastic}} = \sqrt{E_{\text{sum}}/m}$. To elucidate further the effect of $\alpha_0$ and $\tau$ on the frequency of a mode, we choose a constant $E_{\text{sum}} = 1\,\text{MPa}$ and $m = 1\,\text{kg m}^{-1}$ such that $b = 1/\tau$, $c = 1$, $d = \alpha_0/\tau$ and $\omega_{\text{elastic}} = 1\,(\text{krad s}^{-1})$. We expand to second order in $1/\tau$ the real part of $\omega_3$ and obtain

$$\omega_3 \approx 1 - \frac{1}{6\tau^2}\left[1 - \left(\frac{1 - 3\alpha_0}{2}\right)^2\right] + \cdots. \tag{31}$$

The bracket in equation (31) varies between 0 and 1 for all $\alpha_0$ in the interval [1,0], indicating that for large $\tau$, one only expects a decrease in the frequency of the vibrational mode as viscoelasticity increases with decreasing $\alpha_0$.

In summary, in this model, the effect of viscoelasticity on a passing band of the phononic crystal is incorporated by varying the proportions of the viscous and elastic contributions to a SLS model. These proportions are embodied in the parameters $E_\infty$, $E_1$ and $\eta$. We impose the variation in the proportions by keeping the total elastic modulus of the material constant, $E_{\text{sum}} = E_\infty + E_1$, and by varying $\alpha_0$. This means that we are considering a material with a constant effective elastic modulus that is the sum of the moduli of two springs in parallel and vary the modulus associated with the dashpot while keeping the sum constant. As we have seen, in the absence of viscoelasticity the frequency of the passing band of the elastic system is given by $\omega_{\text{elastic}} = \sqrt{E_{\text{sum}}/m}$, and therefore $E_{\text{sum}}$ clearly represents the elastic behavior of the rubber. Reducing $\alpha_0$ to incorporate a viscous effect reduces $E_\infty$ (since $E_\infty = \alpha_0 E_{\text{sum}}$) and increases $\text{E}_1$ (since $E_1 = \alpha_1 E_{\text{sum}}$ and $\alpha_0 + \alpha_1 = 1$) but does not change the overall elastic stiffness of the model, i.e. $E_{\text{sum}}$. Because $E_{\text{sum}}$ is a material's constant, the effect of viscoelasticity through the variation of $\alpha_0$ reduces the frequency as seen in equation (31).

To shed further light on the frequency of the mode of vibration with small values of relaxation time we calculate numerically the frequency of the mode calculated as the sum of the real positive parts of the solutions $\omega_1$, $\omega_2$ and $\omega_3$. In this calculation we again use $m = 1\,\text{kg m}^{-1}$, and $E_{\text{sum}} = 1\,\text{MPa}$. Figure 5 shows that the frequency always decreases with increasing viscoelasticity (i.e. decreasing $\alpha_0$) for all $\tau$ in the range $10^{-2}$ to $10^{-7}$ s. The effect of viscoelasticity on the band structure of a rubber/air phononic crystal can also be understood by considering the frequency-dependent speed of sound of the viscoelastic medium. The phase velocity of sound of a viscoelastic material decreases with decreasing frequency. In the low-frequency regime, for instance, the dispersion curve of the viscoelastic medium is shallower than its elastic counterpart. When inserting inclusions periodically, the band structure of the

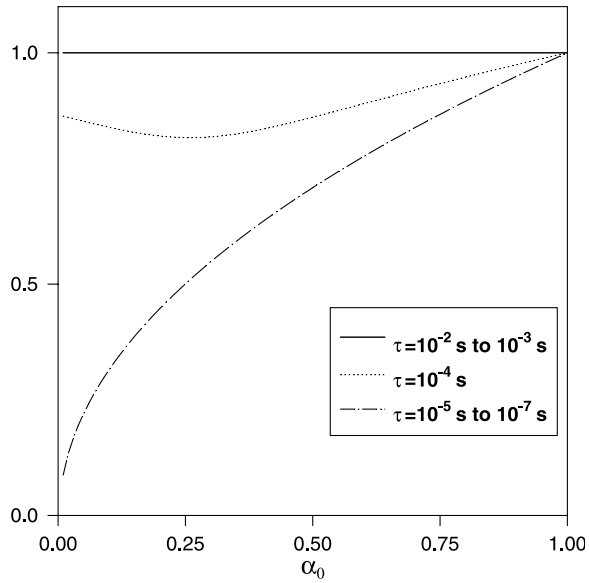


**Figure 5.** Analytical computation of the resonant frequency of the mass/SLS system calculated as the sum of the real positive parts of the complex solutions $\omega_1$, $\omega_2$ and $\omega_3$. as a function of $\alpha_0$ for various values of the relaxation times $\tau$ and $\alpha_0$.

composite can be conveniently constructed by folding the dispersion curve of the homogeneous medium. A gap may then form at the edge of the Brillouin zone. The gap frequency will therefore be expected to be lower for a viscoelastic medium than for the corresponding elastic medium.

## 4. Conclusions

Using the FDTD method developed for modeling 2D elastic and viscoelastic composite structures, we have calculated the transmission spectra of 2D phononic crystals constituted of a square array of cylindrical air inclusions in a solid elastic/viscoelastic rubber matrix. We show that the elastic rubber matrix/air inclusions phononic crystal behaves as a fluid/fluid composite system due to the large contrast between the longitudinal and transverse speeds of sound in rubber. In addition, we pay particular attention to the effect of viscoelasticity on the transmission coefficient of the phononic crystal. We demonstrate that the viscoelasticity coefficients $\alpha_0$ and $\tau$ of a SLS model have an important effect in shifting or highly attenuating the passing bands of the rubber/air phononic crystal. In particular, low-frequency passing bands (less than 2 kHz) shift toward lower frequencies when $\alpha_0$ decreases and the relaxation time $\tau$ is smaller than $10^{-4}$ s. In addition, for relaxation time smaller than $10^{-6}$ s, high frequency passing bands also shift toward lower frequencies. Finally, attenuation increases when $\alpha_0$ decreases and reaches its maximum in the low-frequency band for $\tau = 10^{-4}$ s, and in the high frequency band for $\tau = 10^{-6}$ s. We explain with a one-dimensional viscoelastic analytical model of a single passing band that viscoelasticity may only lead to a decrease in the frequency of the passing bands (and consequently band gaps) in the transmission spectrum of rubber/air systems. Therefore, viscoelasticity offers another degree of freedom in controlling the properties of phononic crystals. Further, the contrast in the longitudinal and transverse speed of sound in rubber/air phononic crystals offers an attractive alternative route (as opposed

to traditional absorptive sound barriers) for designing low-frequency acoustic barriers with frequency tunability via the control of the viscoelastic properties of rubber.

## References


[1] Vasseur J O, Deymier P A, Khelif A, Lambin Ph, Dajfari-Rouhani B, Akjouj A, Dobrzynski L, Fettouhi N and Zemmouri J 2002 *Phys. Rev.* E **65** 056608

[2] Ph. Lambin, Khelif A, Vasseur J O, Dobrzynski L and Djafari-Rouhani B 2001 *Phys. Rev.* E **63** 06605

[3] Vasseur J O, Deymier P A, Frantziskonis G, Hong G, Dajfari-Rouhani B and Dobrzynski L 1998 *J. Phys.: Condens. Matter* **10** 6051–64

[4] Sigalas M, Kushwaha M S, Economou E N, Kafesaki M, Psarobas I E and Steurer W 2005 *Z. Kristallogr.* **220** 765–809

[5] Sigalas M and Economou E N 1993 *Solid State Commun.* **86** 141

[6] Liu Z, Zhang X, Mao Y, Zhu Y Y, Yang Z, Chan C T and Sheng P 2000 *Science* **289** 1734

[7] Psarobas I E 2001 *Phys. Rev.* B **64** 012303

[8] Liu Y, Yu D, Zhao H, Wen J and Wen X 2008 *J. Phys. D: Appl. Phys.* **41** 065503

[9] Laude V, Aoubiza B, Achaoui Y, Benchabane S and Khelif A 2008 *IEEE Int. Ultrasonics Symp. (Beijing, China)* p 2249

[10] Kafesaki M, Sigalas M M and Garcia N 2001 *Photonic Crystals and Light Localization in the 21st Century* ed C M Soukoulis (Dordrecht: Kluwer) p 69

[11] Brandup J and Immergut E H (ed) 1989 *Polymer Handbook* 3rd edn (New York: Wiley)